Can. J. Remote Sensing, Vol. 31, No. 5, pp. 364–376, 2005

Canada-wide foliage clumping index mapping from multiangular POLDER measurements

Sylvain G. Leblanc, Jing M. Chen, H. Peter White, Rasim Latifovic, Roselyne Lacaze, and Jean-Louis Roujean

Abstract. In this paper, vegetation canopy structural information is retrieved over Canada from multiangular Advanced Earth Observing Satellite (ADEOS-1) polarization and directionality of the earth's reflectance (POLDER) data based on canopy radiative transfer simulations using the Five-Scale model. The retrieval methodology makes use of the angular signature of the reflectance at the hot spot, where the sun and view angles coincide, and at the dark spot, where the reflectance is at its minimum. The POLDER data show that the normalized difference hot spot dark spot (NDHD) constructed from the hot spot and dark spot reflectances has no correlation with the nadir-normalized normalized difference vegetation index (NDVI), from which vegetation properties are often inferred, indicating that this angular index has additional information. Five-Scale simulations are used to assess the effects of foliage distribution on this angular index for different crown sizes, spatial distribution of crowns and foliage inside crowns, and foliage density variations. The simulations show that the NDHD is related to canopy structure quantified using a clumping index. This latter relationship is further exploited to derive a Canada-wide clumping index map at 7 km by 7 km resolution using spaceborne POLDER data. This map provides a critical new source of information for advanced modelling of radiation interaction with vegetation and energy and mass (water and carbon) exchanges between the surface and the atmosphere.

Résumé. Dans cet article, on extrait l'information structurale du couvert de végétation au-dessus du Canada à partir de données multi-angulaires POLDER de ADEOS-1 basé sur des simulations du modèle de transfert radiatif Five-Scale. La méthodologie d'extraction utilise la signature angulaire de la réflectance au point anti-spéculaire (hot spot), où les angles solaire et de visée se rencontrent, et au point sombre (dark spot), où la réflectance est à son minimum. Les données POLDER montrent que le NDHD (« normalized difference hot spot dark spot ») construit à partir des réflectances au point anti-spéculaire et au point sombre n'est pas corrélé au NDVI normalisé au nadir, à partir duquel les propriétés de la végétation sont souvent déduites, indiquant que cet indice angulaire contient plus d'information. Les simulations de Five-Scale sont utilisées pour évaluer les effets de la répartition du feuillage sur cet indice angulaire pour différentes dimensions de couronne, la répartition spatiale des couronnes et du feuillage à l'intérieur des couronnes et les variations de densité du feuillage. Les simulations montrent que le NDHD est relié à la structure du couvert quantifiée par le biais d'un indice d'agrégation. Cette relation est exploitée davantage pour dériver une carte d'indice d'agrégation à l'échelle du Canada à une résolution de 7 km × 7 km utilisant des données satellitaires POLDER. Cette carte fournit une nouvelle source critique d'information pour la modélisation avancée des interactions du rayonnement avec la végétation et des échanges d'énergie et de masse (eau et carbone) entre la surface et l'atmosphère.
[Traduit par la Rédaction]

Introduction

Quantitative assessment of vegetation properties from satellite imagery has matured greatly in recent years. Many retrieval techniques now exist to quantify vegetation density and vigour. However, the remote sensing information used in these techniques is usually based on single-view reflectance, particularly in considering vegetation indices such as the normalized difference vegetation index (NDVI). The vegetation amount is well characterized by the leaf area index (LAI), which gives an estimate of the foliage surface per unit of ground surface. The LAI retrieval is achieved from different remote sensing sensors and different methods (Myneni et al., 1997; Chen et al., 2002; Privette et al., 2002; Roujean and

Received 4 February 2005. Accepted 14 June 2005.

S.G. Leblanc.[1] Canada Centre for Remote Sensing (CCRS), Natural Resources Canada, Centre spatial John H. Chapman, 6767 Route de l'aéroport, St. Hubert, QC J3Y 8Y9, Canada.

J.M. Chen. Department of Geography and Program in Planning, University of Toronto, 100 St. George Street, Room 5047, Sidney Smith Hall, Toronto, ON M5S 3G3, Canada.

H.P. White and R. Latifovic. Canada Centre for Remote Sensing (CCRS), Natural Resources Canada, 588 Booth Street, Ottawa, ON K1A 0Y7, Canada.

R. Lacaze. Medias-France, CNES-BPI 2102, 18, av. Edouard Belin, 31401 Toulouse Cedex 04, France.

J.-L. Roujean. Météo-France, CNRM, 42, avenue G. Coriolis, 31057 Toulouse Cedex, France.

[1]Corresponding author (e-mail: Sylvain.Leblanc@CCRS.NRCan.gc.ca).

Lacaze, 2002; Fernandes et al., 2003). In most situations, a random distribution of the LAI is assumed within the pixel area. Occasionally, land cover segmentation is used with different relationships to compensate for the structural and spatial patterns of different vegetation types. As canopy structure varies even within a given vegetation type, however, land cover segmentation is not always sufficient for LAI retrieval. Therefore, it seems necessary to use additional information. A complement to single-look and nadir optical data is to consider multiangular sensor systems such as the multiangular imaging spectroradiometer (MISR) onboard the TERRA satellite and Advanced Earth Observing Satellite (ADEOS-1) polarization and directionality of the earth's reflectance (POLDER) that acquire multiple view angle reflectance on a single orbit. Asner (2000) showed early results of the advantage of using angular measurements for land applications. Some studies have incorporated the angular signature or non-nadir data into LAI retrieval (Bicheron and Leroy, 1999; Knyazikhin et al., 1998), and other studies have shown the potential of angular measurements in retrieving information about foliage organization (Lacaze et al., 2002; Leblanc et al., 2002; Pinty et al., 2001, Widlowski et al., 2001). The heterogeneity of the foliage distribution can be quantified by a clumping index based on Beer–Lambert's law (Nilson, 1971):

$$P(\theta) = \exp\left[\frac{-G(\theta)\Omega(\theta)L}{\cos\theta}\right], \tag{1}$$

where $(P\theta)$ is the gap fraction at view zenith angle θ, L is the leaf area index, $(G\theta)$ is the projection of unit leaf area in the θ direction, and $\Omega(\theta)$ is the clumping index. $\Omega(\theta)$ greater than unity implies that the foliage is regularly distributed, $\Omega(\theta) = 1$ represents a random distribution, and $\Omega(\theta)$ less than unity implies that the foliage is clumped. The clumping index is generally found as follows:

$$\Omega(\theta) = \frac{\ln[P_c(\theta)]}{\ln[P_r(\theta)]} = \frac{L_e(\theta)}{L} \tag{2}$$

where $P_c(\theta)$ is the gap fraction measured in the clumped canopy; $P_r(\theta)$ is the theoretical gap fraction from Equation (1), with $\Omega(\theta) = 1$; and $L_e(\theta)$ is the so-called effective LAI (Chen and Cihlar, 1995) that represents the LAI obtained from inversion of Equation (1) without clumping considerations such as $L_e(\theta) = \Omega(\theta)L$. Although LAI mapping is often performed from remote sensing data, some empirical data and model simulations have shown that the nadir remote sensing signal may be more related to the effective LAI, or the gap fraction, than to the LAI (Chen and Cihlar, 1996; Leblanc et al., 2002). To retrieve a more precise LAI from remote sensing data, the clumping index may be needed.

The gap fraction can easily be estimated from optical instrument data such as hemispherical photographs (e.g., Leblanc et al., 2005), whereas the LAI is a more difficult parameter to measure. Although Equation (1) is a simplified expression of the complexity of light transmittance through a canopy, it is usually adequate for direct light transmittance and is the basis of field optical LAI retrieval (e.g., Lang and Xiang, 1986; Chen and Cihlar, 1995; Leblanc et al., 2005). For needleleaf species, the clumping index is usually separated into two components, namely clumping at a scale larger and smaller than the shoot:

$$\Omega(\theta) = \frac{\Omega_E(\theta)}{\gamma_E} \tag{3}$$

where $\Omega_E(\theta)$ is the clumping of foliage elements, leaves for broadleaf species and shoots for needleleaf species; and γ_E is the ratio of needles to shoots, which accounts for clumping of needles into shoots (Chen et al., 1997). The following different methods have been used for in situ estimation of the clumping index $\Omega_E(\theta)$ in vegetated canopies: (*i*) measurement of the LAI with allometric relationships compared with the effective LAI obtained with optical instruments (Kucharik et al., 1997) using Equation (2), which allows $\Omega(\theta)$ to be estimated directly but generally with the assumption that the foliage elements are randomly oriented, i.e., $G(\theta) = 0.5$; (*ii*) the finite-length averaging method applied to optical instruments (Lang and Xiang, 1986; Leblanc et al., 2005) in which a logarithmic averaging of the gap fraction scheme is used over finite lengths in the inversion of Equation (1), compared with the logarithm of the mean gap fraction (effective LAI); (*iii*) the gap size accumulation distribution method applied to optical instruments (Chen and Cihlar, 1995; Leblanc, 2002) in which large gaps that contribute to the gap fraction but are not possible in a random foliage distribution are removed from the gap fraction based on a theoretical random gap size distribution; and (*iv*) the Piélou aggregation index applied to optical instruments (Walter et al., 2003) in which sequences of gaps and nongaps are used to infer the clumping index.

The clumping index can be used to improve the modelling of the carbon cycle, as it allows a better segmentation of the solar radiation distribution in sunlit and shaded leaves as compared to models that relate carbon absorption to the intercepted solar radiation only (Chen et al., 2003). Several studies (Du Pury and Farquhar, 1997; Wang and Leuning, 1998; Chen et al., 1999b; Liu et al., 2002) favour using a sunlit – shaded leaf separation based on Norman (1993) for canopy-level photosynthesis simulations and thus require the clumping index. Previous studies have used a constant clumping index for a given land cover type, associated with LAI based on remote sensing (e.g., Liu et al., 1997). It has been shown that clumping index variation for a given effective LAI can have important effects on the gross and net primary productivity of a forest stand (Chen et al., 2003). Previous studies have shown that the multiangular measurement is related to the clumping index (Lacaze et al., 2002; Chen et al., 2003). Based on these studies, the goal of this paper is to develop an algorithm for mapping the clumping index for Canada from POLDER multiangular reflectance. The hot spot, where sun and view geometry

coincide, and the dark spot, where the reflectance is at its minimum (see **Figure 1**), form the basis of retrieving the clumping index from the angular signature.

Material and method

Data

Data from the POLDER sensor onboard the ADEOS-1 Japanese platform are used in this study by virtue of the ability of the sensor to measure the same ground surface (pixel) at up to 14 viewing angles during a single overpass under clear sky conditions (Deschamps et al., 1994). The POLDER sensor is a push-broom charge-coupled device (CCD) matrix with a wide field of view lens (114°) that gives a swath of about 2400 km, which allows the same ground area to be viewed during successive orbital passes. Because of this high frequency of revisiting sequence, the directional space is well covered after a few days, thereby increasing the chances of sampling the hot spot phenomenon. POLDER nadir pixel size is 6 km by 7 km, but we use a grid of 7 km by 7 km in this study to account for footprint consideration, since the multitemporal registration is estimated at 0.3 pixels (Leroy et al., 1997).

Reprocessed POLDER data using the sea-viewing wide field-of-view sensor (SeaWiFS) OC2-v4 algorithm (Fougnie et al., 2001) are used in this study. ADEOS-1 failed at the end of June 1997, and therefore only the data from 15 to 30 June are used to get as closed as possible to the peak growing season conditions within Canada. Although POLDER data are available in several bands, the present study employs directional data from the near-infrared (NIR) band (centred at 865 nm) for the following reasons: (*i*) more consistent reflectance values are obtained at NIR than at visible wavelengths due to reduced atmosphere absorption and scattering (e.g., Fernandes et al., 2003), (*ii*) better fit of bidirectional distribution function (BRDF) kernel models to NIR directional data with a high coefficient of determination (R^2) and low root mean square error (RMSE) (Leblanc et al., 2002), and (*iii*) reduced specular effect on NIR reflectance of water bodies that are very common within the Canadian landmass at 7 km by 7 km resolution (Lacaze, 1999; Pavlic et al., 2002).

Data processing

Within POLDER, pixel cover type composition was determined using a 1998 land cover map of Canada derived from Système Pour l'Observation de la Terre (SPOT-4) VEGETATION 1 km spatial resolution data (Cihlar et al., 2002.). The land cover map was resampled into spatial resolution equivalent to POLDER data using a non-overlapped 7 by 7 running window. Each 7 km by 7 km pixel was characterized with the dominant cover type. The running window was also used to estimate the percent cover of needleleaf species in the POLDER pixel. The needleleaf percentage was calculated based on all pixel types in the 7 by 7 windows, not just the dominant type. Pixels with cover type described as high conifer content were assumed to be 100% conifer, and mixed pixels were given the value of 50%. Even with these assumptions, less than 3% of the land pixels are pure conifers at 7 km resolution. For each of the 7 km by 7 km pixels, the centre coordinate is transformed into the nearest POLDER grid position and an automated routine searches for all POLDER measurements available for the given period (15–30 June 1997). Up to 200 reflectance values from different view and solar geometries are extracted for a single pixel coordinate.

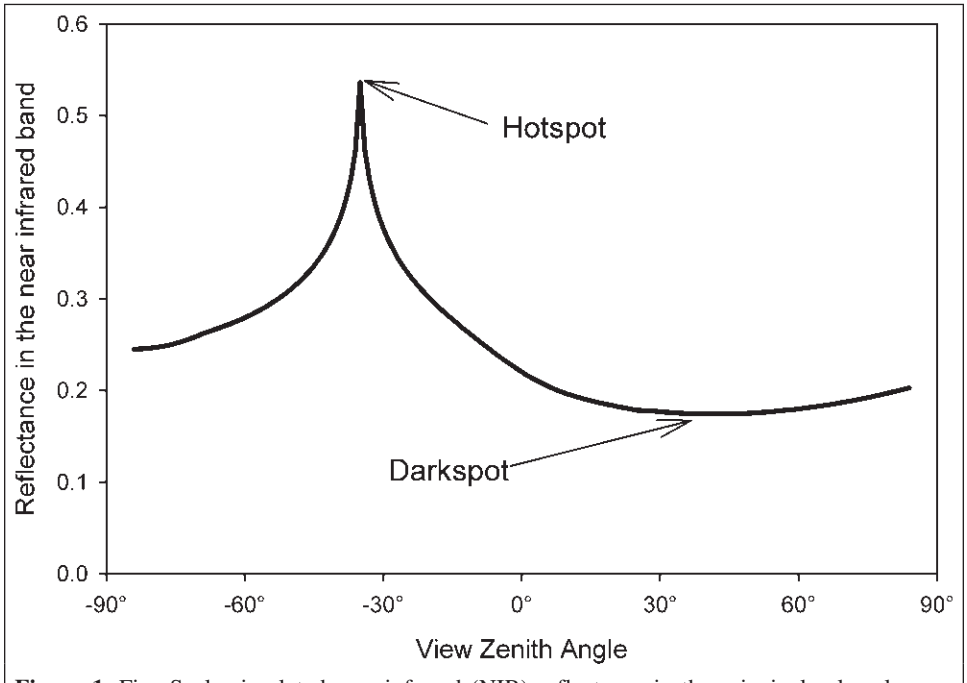

Figure 1. Five-Scale simulated near-infrared (NIR) reflectance in the principal solar plane.

Five-Scale model

Foliage density and distribution can significantly alter the remote sensing signal. Moreover, foliage clumping is a characteristic that can occur at different scales. The present study encompasses clumping at the shoot, branch, crown, and distribution of crown scales levels, corresponding to the four scales of the Four-Scale canopy radiative transfer model (Chen and Leblanc, 1997). The latest version of the model is used and is now called Five-Scale (Leblanc and Chen, 2000). Five-Scale is a combination of the Four-Scale and LIBERTY (Dawson et al., 1998) models. The ability of Five-Scale to reproduce directional reflectance has been validated with PARABOLA (Chen and Leblanc, 1997) and airborne POLDER data (Leblanc et al., 1999). Five-Scale is a geometric–optical canopy radiative transfer model. It simulates the directional reflectance of forest canopies using crowns as geometric objects such as cylinder and cone for conifers and spheroid for deciduous. These geometric objects are composed of foliage elements that can be grouped to form branches. The complex solar radiation multiple scattering of plant canopies is simulated with view factors that allow calculation of the amount of radiation reaching shaded portions and the enhancement of sunlit portions of the canopy and background (Chen and Leblanc, 2001). Five-Scale is used here to relate the LAI, clumping index, and other canopy architectural parameters to the canopy directional reflectance. The foliage clumping index is not a Five-Scale input parameter. The index $\Omega(\theta)$ is calculated based on Equation (2), where $P_c(\theta)$ is the clumped canopy gap fraction as calculated by Five-Scale, and $P_r(\theta)$ is the random canopy gap fraction computed with Beer-Lambert's law (Equation (1), with $\Omega(\theta) = 1$). Five-Scale completely separates orientation effects of clumping and foliage elements, i.e., $G(\theta)$ is completely independent of $\Omega(\theta)$. Angularly independent foliage clumping at the branch level can be entered as an input parameter (Ω_B), or a branch architecture can be used to simulate the clumping of foliage in branches. The clumping of needles into shoots is assumed to be angularly independent and is quantified by the ratio of needles to shoots γ_E (Chen et al., 1997). To remove species bias that may be found by using specific optical and canopy structures variables, the simulations were performed with different optical factors for background and foliage and canopy structures, which encompass more than the naturally occurring conditions in Canada. Twenty-two sets of optical properties are used, corresponding to different cases of red and NIR bands (see **Table 1**). However, the focus in this study is on the NIR band simulations.

FLAIR model

Although Five-Scale is computationally efficient, it is still too slow for inversion or to fit large angular datasets. Look-up-table or neural network methods could be used but are not necessary for the purpose of this study. Instead, the Four-Scale linear model for anisotropic reflectance (FLAIR) (White et al., 2001b; 2002) is used to parameterize the BRDF of all POLDER pixels. FLAIR is a linear kernel-like model developed from the Four-Scale model (Chen and Leblanc, 1997). Although simplifications were performed in developing FLAIR, efforts were also made not to limit the model to specific canopy characteristics while maintaining direct relationships between canopy architecture and model coefficients. This has resulted in a model with five descriptors of the canopy: multiple scattering factors at foliage and background level, reflectivity of foliage and background, and the canopy gap fraction relative to the effective LAI. FLAIR applications were demonstrated in White

Table 1. Five-Scale model input parameters for forest simulations.

Parameter	Value used in simulations
Density (no. of stems/ha)	500, 750, 1000, 2000, 3000, 4000, 6000
Leaf area index, LAI	0.5, 1.0, 2.0, 3,0, 4.0, 5.0, 6.0, 7.0, 8.0, 10.0, 12.0
Needle to shoot ratio (shoot clumping), $\gamma_{\backslash 45}$	1.0 (deciduous), 1.4 (coniferous)
Crown shape	Spheroid, cone + cylinder
Foliage clumping in branches, Ω_B	0.8, 1.0 (no clumping)
Tree clumping, m_2	No clumping, 10
Crown height, H_b (m)	5, 10, 20, 40
Crown base height, H_a (m)	0.0, 10.0
Crown radius, R (m)	0.5, 0.7, 1.0, 2.0, 3.0, 5.0
Foliage orientation, α_L (°)	Random, 75, 25
Branch orientation, α_B (°)	Random, 75, 25
Background reflectivity	
NIR	0.15, 0.35
Red	0.05, 0.10
Foliage reflectivity	
NIR	0.35, 0.50, 0.60
Red	0.05, 0.10, 0.15
Foliage transmittance	
NIR	0.35, 0.45
Red	0.05, 0.15

Note: Symbols refer to those used in Chen and Leblanc (1997) and Leblanc et al. (1999).

Table 2. Angular indices from the literature.

Index	Formula	Reference
Anisotropy index, ANIX	$ANIX = \rho_{Max}/\rho_{Min} = \rho_H/\rho_D$	Sandmeier et al., 1998
Hot spot dark spot index, HDS	$HDS = (\rho_H - \rho_D)/\rho_D = ANIX - 1$	Chen et al., 1999a; 2003; Lacaze et al., 2002
Normalized difference hot spot dark spot, NDHD	$NDHD = (\rho_H - \rho_D)/(\rho_H + \rho_D) = (ANIX - 1)/(ANIX + 1)$	Leblanc et al., 2001; 2002; Nolin et al., 2002

Note: ρ_{Max} and ρ_{Min} are the maximum and minimum measured reflectances, respectively. ρ_H and ρ_D are the hot spot and dark spot reflectances, respectively.

et al. (2001a; 2002). A FLAIR version with six free parameters is used here, where the effective LAI is replaced by the true LAI and the clumping index.

FLAIR was originally developed to be inverted using the simplex method (White et al., 2001b). The Powell method (Press et al., 1994) is used to retrieve the six FLAIR parameters. A negative merit function was used when reflectivity and proportion parameters were outside the 0–1 range and when the shaded foliage and background excitance were larger than half that of their sunlit counterparts. By using the FLAIR-retrieved parameters and resimulating the full BRDF at a common solar zenith angle, the hot spot and dark spot reflectances can be obtained to calculate any of the anisotropic indices listed in **Table 2**. Based on previous simulated tests (Leblanc et al., 2002), only the normalized difference hot spot dark spot (NDHD) is used because it showed a more linear relationship with the clumping index when fixed optical properties are used.

Results and discussion

Normalization and extrapolation

As previously stated, the POLDER acquisition design gives a wide range of view angles for a given ground area, up to more than 200 for the data used here. Nevertheless, it does not allow the hot spot to be found for all pixels, especially within a short time span. FLAIR is used here as a normalization and extrapolation tool to obtain the reflectance at any sun and view geometries from the available POLDER data. For this study, the angles of interest correspond to the reflectance at the hot spot, the dark spot, and the nadir geometries, all normalized at a common solar zenith angle (SZA) of 35°, which is representative of the mean SZA for Canada during the month of June. The hot spot and nadir reflectance values are found by simulating the reflectance at the exact angular geometry. The theoretical dark spot is found as the lowest simulated reflectance on the forward-scattering part of the principal solar plane for a view zenith angle of less than 65°, but for our purposes using a fixed geometry dark spot at 60° or letting the dark spot angle varies makes negligible differences.

Figure 2a shows how the largest reflectance values, which are usually found near the hot spot, are transformed by FLAIR into the hot spot reflectance at SZA of 35°. FLAIR-normalized reflectance values are more often larger than the highest measured reflectance values. The values most affected by the FLAIR normalization are from pixels where none of the view

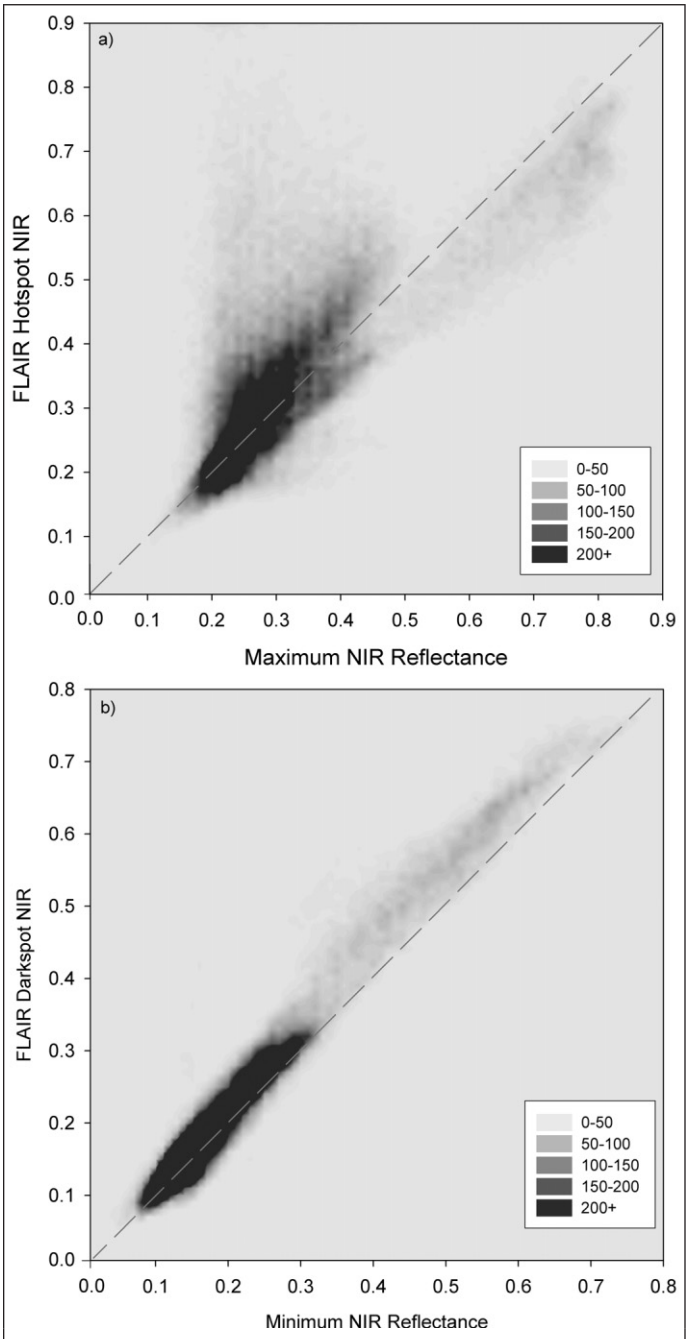

Figure 2. Effect of the FLAIR normalization at the (a) hot spot and (b) dark spot on the POLDER data. The FLAIR dark spot is found from view zenith angle less than 65°.

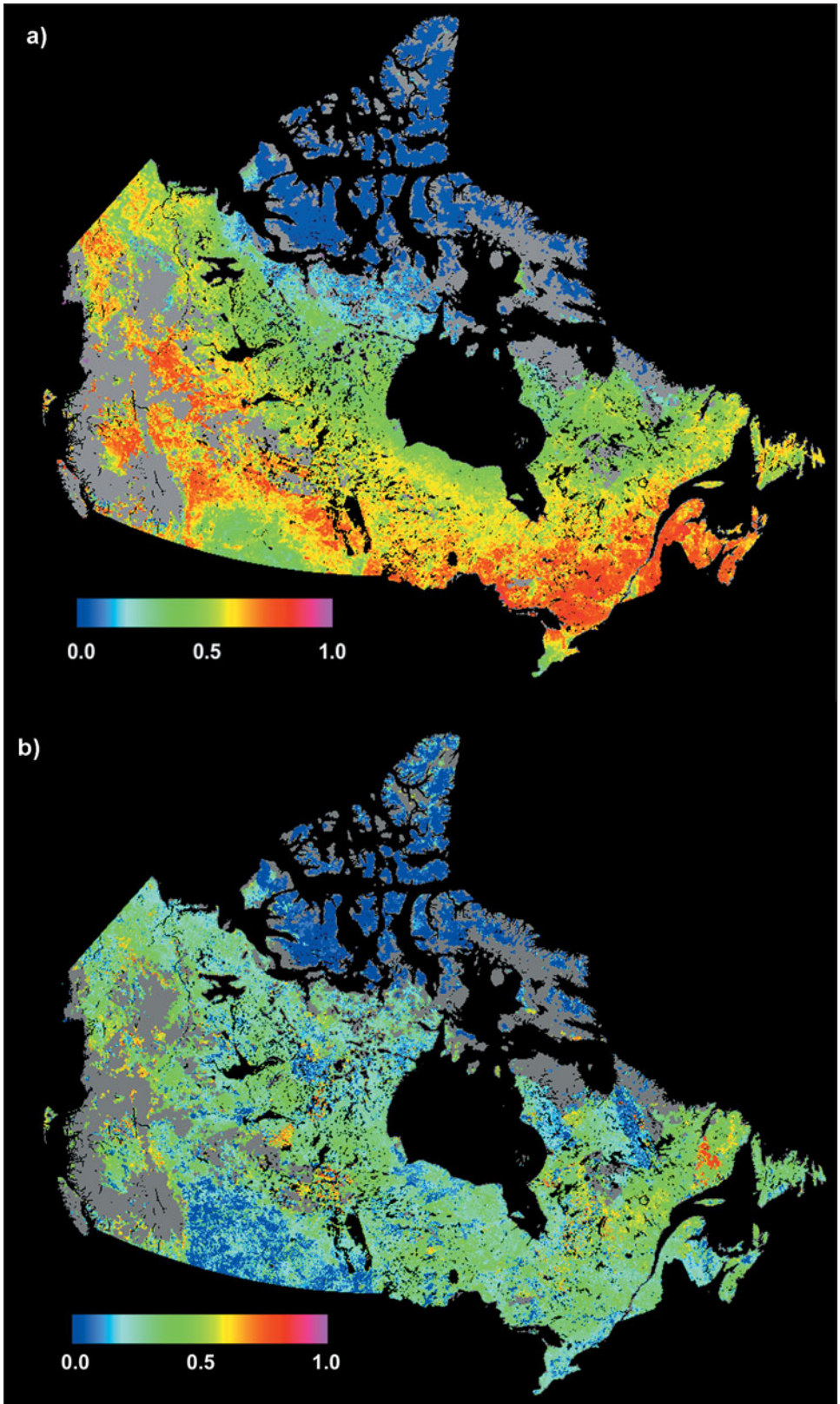

Figure 3. (a) FLAIR nadir normalized NDVI, where negative NDVI values from ice surfaces have been set to zero. (b) NDHD from FLAIR extracted hot spot and dark spot. POLDER data, 15–30 June 1997. The grey areas are pixels without data.

zenith angles were in the vicinity of the hot spot. Some values may have been either decreased or increased when a hot spot value was found because the POLDER data were from SZA greater or smaller than 35°. **Figure 2b** has the dark spot normalization effect. The dark spot normalization has less effect than the hot spot normalization because the reflectance does not vary much in the forward-scattering angular space for a given surface. Nadir normalization was also performed for both red and NIR bands, but these results are not shown because they are similar to the dark spot normalization shown in **Figure 2b**. Both nadir and dark spot reflectances are less affected by the normalization effects than the hot spot reflectances.

Remote sensing information content

Information in coarse-resolution remote sensing data is represented by the spectral, spatial, and temporal components. The dimensionality of spectral components is often reduced through band combinations, i.e., reflectance index. **Figure 3a** shows one of the most frequently used vegetation indices, the NDVI, based on the NIR and red bands of the POLDER data normalized at nadir and SZA of 35° by FLAIR. The largest NDVI values are found in very dense vegetated areas, mainly where broadleaf species are found. To visualize the directional information and to remove some of the effects of the different optical properties of the foliage and background, the NDHD index is calculated for the hot spot and dark spot reflectances extracted with FLAIR. Other angular indices have been used previously (see **Table 2**), but they are all mathematical transformations of each other. **Figure 3b** shows the resulting NDHD map. The prairies and far north generally have the lowest NDHD values, indicating very isotropic surfaces, and the forested areas have NDHD values close to 0.5. Overall, the NDHD values for broadleaf species are not that different from those for coniferous species. The NDVI map has smoother variations than the NDHD map. This behaviour can be explained in part by the extrapolation of the hot spot for pixels where the acquisition geometry did not get close to the hot spot, or it could be due to changes in the vegetation over the 2 weeks of measurements for the northern areas, as the vegetation vigour is still changing rapidly in those areas because the growing season starts later than it does in southern Canada. Moreover, the central Canada growing season started late in 1997, with leaf emergence around mid-May near Ottawa (Leblanc and Chen, 2001).

Figure 4 shows that the FLAIR-normalized nadir NDVI is not related to the FLAIR-normalized NDHD from the NIR band. This indicates that the information contents of these two indices are different. By using FLAIR to normalize and extrapolate the POLDER data to hot spot, dark spot, and nadir reflectances, smooth variations of the reflectance were generally found, indicating that FLAIR is good at assimilating data and reproducing physically valid reflectance. Moreover, FLAIR fits to the POLDER data also gave parameters such as LAI and clumping index directly. The retrieved values didn't seem to be consistent over Canada's landmass, however, and thus were not investigated in more detail in this study.

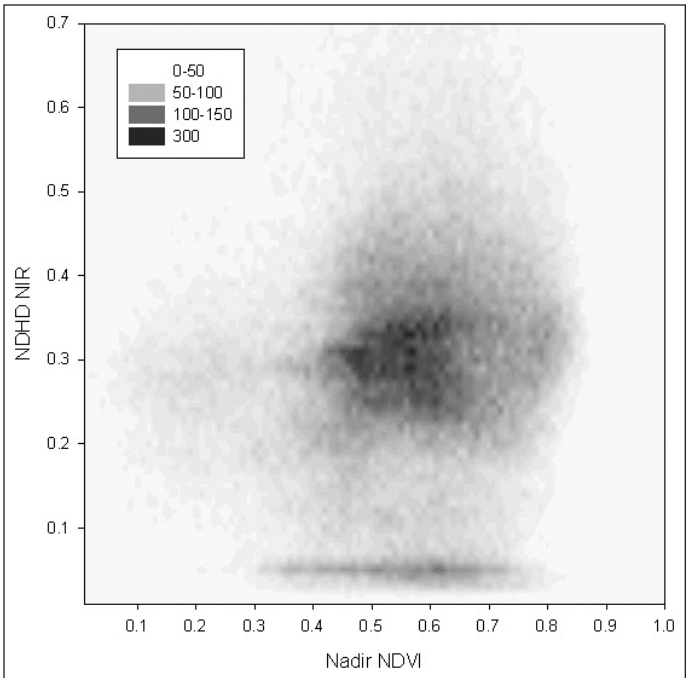

Figure 4. Relationship between the NDVI and the angular index NDHD based on the non-ice POLDER data over Canada (**Figures 3a** and **3b**) from 15–30 June 1997.

Simulation results

In this study, it is supposed that a large set of Five-Scale simulations can help in assessing the relationship between clumping index and angular properties of directional reflectance. The set of simulated parameters is large (see **Table 1**), but not continuous, and covers much more than the typical Canadian vegetation characteristics. Additional simulations were performed for low vegetation such as grassland and agriculture, which are included in the broadleaf results. Although Five-Scale was not designed for nonforested area, grass-like simulations can be obtained by using large numbers of small stems. Simulations with 500 000 – 1 000 000 stems per hectare and 0.01–2.00 m high with radius of 0.01–0.12 m were performed for LAI from 0.10 to 3.00. The simulation sets were run over many months and are combined to show the relationship between the clumping index and directional measurements. **Figures 5a** and **5b** show the relationship between clumping index and the hot spot and dark spot, respectively. Both red and NIR bands (based on **Table 1** input optical parameters) are shown. The analysis of simulated data did not provide evidence that the clumping index is directly related to the hot spot. However, there is some evidence that relationships between clumping index and dark spot exist because clumped canopies, i.e., dense tree crowns, branches, shoots, etc., cast dark shadows and decrease the dark spot reflectance. Two relationships can be seen in **Figure 5b**: one for the red band and one for the NIR band. Because of natural

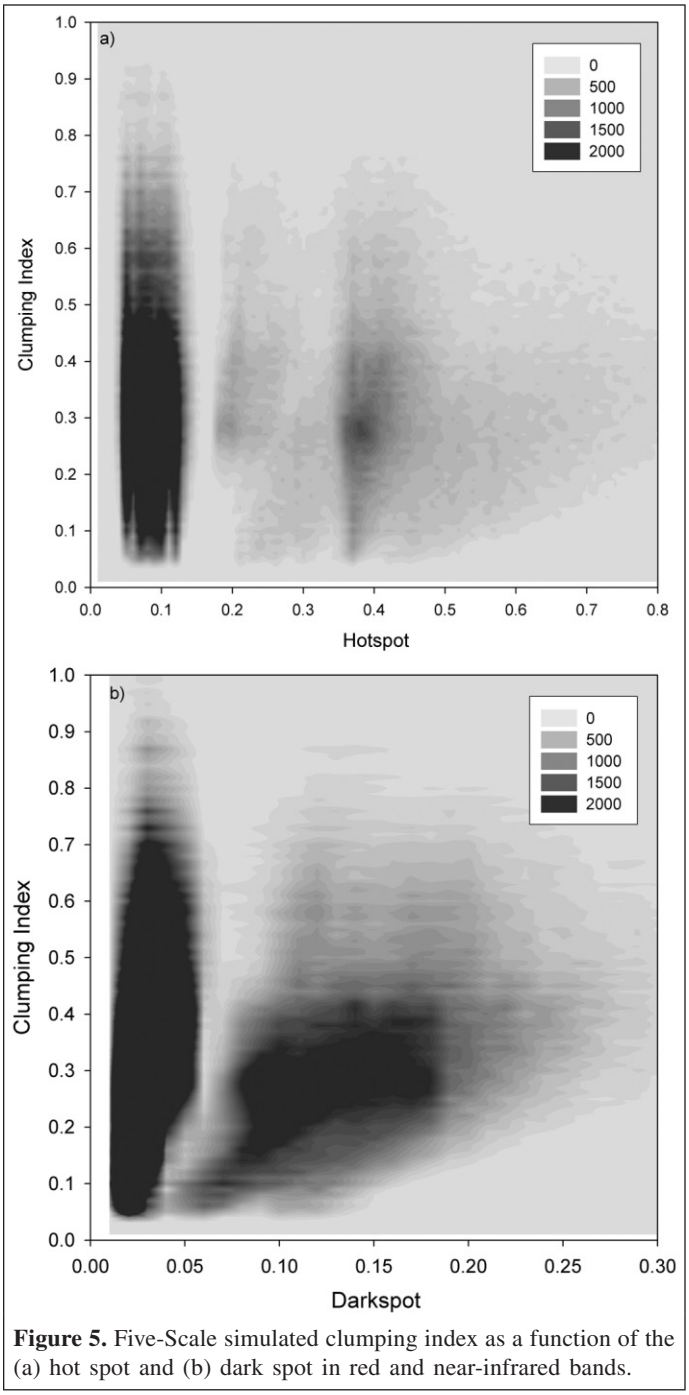

Figure 5. Five-Scale simulated clumping index as a function of the (a) hot spot and (b) dark spot in red and near-infrared bands.

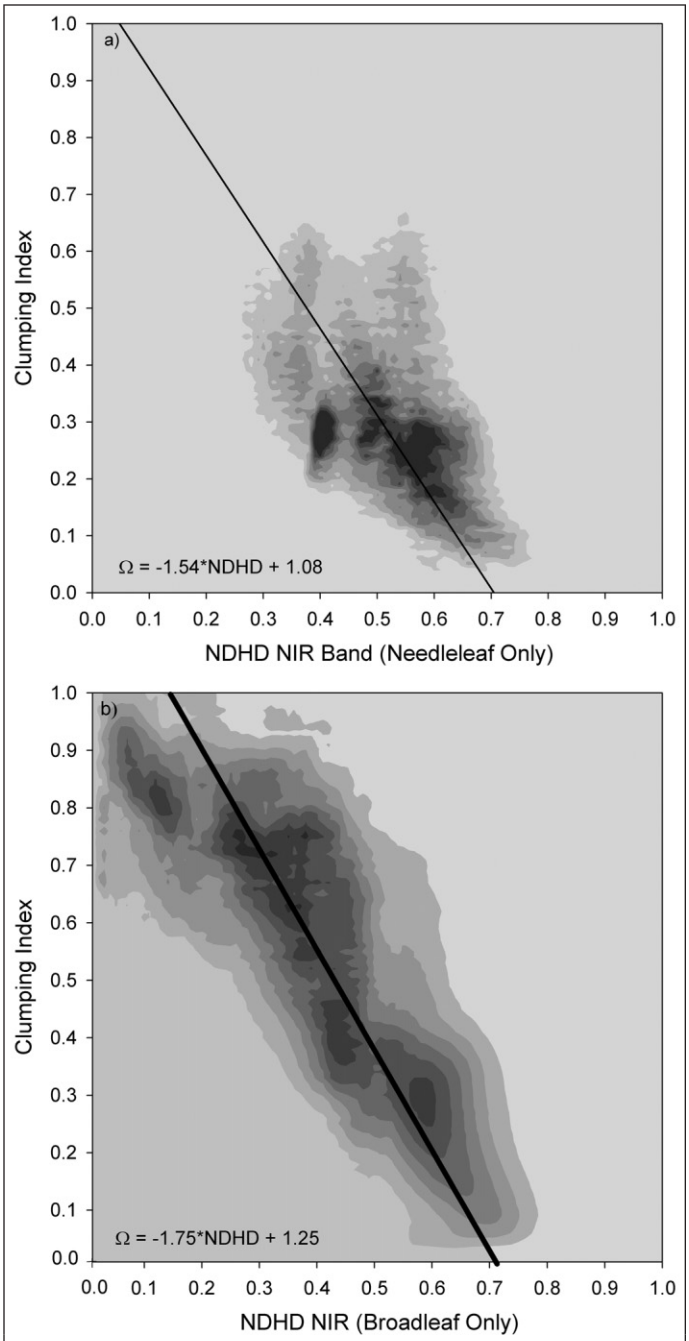

Figure 6. Five-Scale simulated relationships between near-infrared NDHD and the total foliage clumping index (Ω) for (a) needleleaf forests and (b) broadleaf forests and grassland.

variations in foliage optical properties, however, it seems more appropriate to use a normalized index such as NDHD. The clumping index information seems to be in the dark spot reflectance, whereas the hot spot can be seen as the normalizing factor when used in the NDHD.

Figures 6a and **6b** show the relationship between NDHD and the clumping index for coniferous and deciduous species, respectively. For clumping index values for low-density coniferous species, all simulations converge to a clear relationship, but at high clumping index values, for canopies with a more random foliage distribution, the relationship is not as clear. The relationship could have been improved by using more γ_E values. Only one case of needle clumping with $\gamma_E = 1.4$ was used in the simulation sets to save computational time, forcing the clumping index values to be lower than 0.7 (**Figure 6b**). The large scatter in **Figures 6a** and **6b** is due in large part to the large set of input parameters used for the simulations. The combinations of input that give very low foliage density in the crowns (<0.001 m^3/m^2), large vertical overlap crowns (>400%), and low canopy closure (<10%) were rejected. A robust

Table 3. Five-Scale NDHD clumping index fit values A and B ($\Omega = A \times \mathrm{NDHD} + B$).

Class	A	B
Conifer	–1.54	1.1
Broadleaf	–1.75	1.3

regression (Fernandes and Leblanc, 2005) is used to find a relationship between the NDHD and the clumping index. In this kind of regression, the median of the slopes and y-intercept are used instead of the mean values that are generally found in least-square regressions. This allows the regression line to be less influenced by outliers compared to a classical linear regression. Relationships for broadleaf and needleleaf species are found. The intercept and slope of the two linear relations are listed in **Table 3**. The following equation is used to apply these relationships to the POLDER data:

$$\Omega(35°) = [XA_C + (1-X)A_B]\mathrm{NDHD}(35°) + [XB_C + (1-X)B_B] \quad (4)$$

where X is the percentage of the pixel covered with needleleaf species; the constants A and B (**Table 3**) are found with the Five-Scale simulations; and the subscripts B and C denote broadleaf and coniferous, respectively.

Clumping index map

The POLDER dataset used in this study has large coverage gaps over Canada (25%), due most probably to cloud cover in June 1997. Thus to obtain a complete map of Canada, these pixels are filled with averaged NDHD values from the most frequently occurring cover type based on 40 spectral classes that were used to create the 12-class SPOT VEGETATION land cover map. Moreover, areas where the hot spot is farther than 10° from the closest measurements are discarded because of the uncertainties in extrapolating the hot spot; these are also replaced by the mean NDHD for the corresponding spectral classes. We used the spectral classes instead of the land cover type to have a more regional distribution of the clumping index. **Figure 7** shows the resulting clumping index map based on Equation (4) applied to the FLAIR-normalized POLDER NDHD. Northern, grass, and agricultural areas have a clumping index near unity. At the scale of the POLDER data, it is a very difficult, if not impossible, task to validate such a product. Contrary to near-nadir (or normalized to nadir) remote sensing, there is no sensor available at the moment at a resolution that

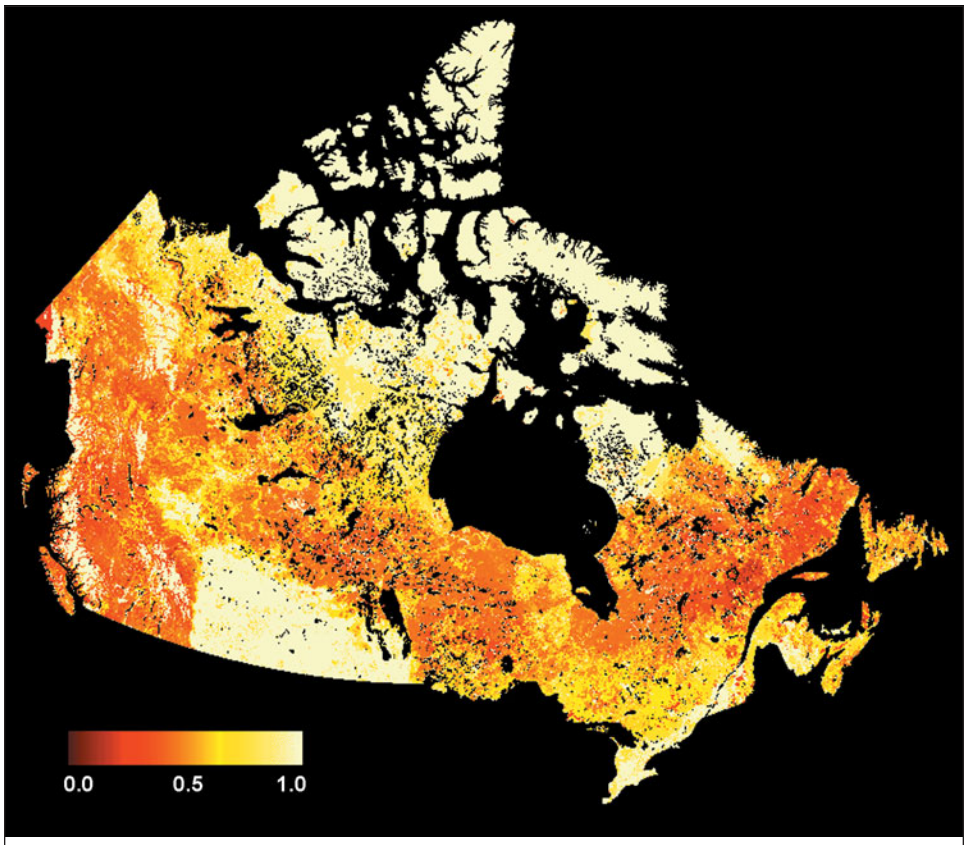

Figure 7. Clumping index map based on the NDHD POLDER based data from **Figure 3b** and a SPOT VEGETATION based land cover map. Only the pixels where the reflectance was measured within less than 10° from the hot spot were kept from **Figure 3b**; the remaining land pixels were filled with mean values from the associated cover type based on the land cover map. Values greater than unity were assigned a clumping index of one.

could be used as an intermediate scale. Sensors such as CHRIS on the PROBA platform, with a pixel resolution of the order of a plot (25–50 m), have multiangular view capabilities, but the angular sampling is not adequate for characterization of the hot spot for a given area because it has only five viewing angles (Barnsley et al., 2000). Airborne POLDER data were compared with field measurements in Lacaze et al. (2002), but with only five data points. The most clumped area is found in eastern Canada, on the north shore of the St. Lawrence River in the province of Quebec and in Labrador. **Figure 8** shows the statistical distribution of the retrieved clumping index values for pixels with vegetated cover types and with reflectance acquired within 10° of the hot spot. Clumping index values vary from near-random for broadleaf species (**Figure 8a**), with 86% of the values from 0.60 to 1.00, to more clumped for mixed broadleaf–needleleaf species (**Figure 8b**), with 85% of the values from 0.50 to 1.00, and to very clumped for needleleaf species, with 85% of the values from 0.35 to 0.60 (see **Figure 8c**). This is in agreement with measured clumping index values in boreal forests, as some black spruce stands have been shown to have a clumping index as low as 0.30, whereas deciduous species generally have values of between 0.70 and 0.90 (see **Table 4**). The averaged clumping index based on pixels with a reflectance acquired within 10° of the hot spot is not changed much if only pixels with a hot spot within 5° are used; all cover types are affected by at most a 1% relative change, except for the closed deciduous and mixed forests, which are increased by 3.6% and 2.0%, respectively. Although uncertainties from both the data and simulations affect the resulting clumping index values, the retrieved values are within the physically possible range. The retrieved dark spot should have a high accuracy, estimated at about 2% error based on **Figure 2**, and the hot spot may be estimated at around 5%. This implies that the retrieved NDHD has error at about 14% for the pixels with reflectance closer than 10°. The error for the relationship between clumping index and NDHD is more difficult to assess because we used a very large set of input variables. Previous Five-Scale simulation sets have shown better relationships between the clumping index and NDHD (Chen et al., 2003), since the input data were specific to a given species. We chose a larger set here to have less biased relationships, but at the cost of having less precise maps. Moreover, the relationships are dependent on the percentage of conifer in the pixels, adding another level of uncertainty to the final clumping index values. There is a difference of less than 15% between the factors found for the deciduous and coniferous relationships (**Table 3**). If we combined this with the error for the data, we get about 30% error for the retrieved clumping index. Ecological models have used a fixed clumping index value of 0.5 for coniferous forests (Liu et al., 1999), and this value has a root mean square difference of only 0.11 (22%) with the clumping index retrieved for pixels with 75% needleleaf, less than the estimated error of 30%.

Conclusions

Through canopy radiative transfer simulations and POLDER data analysis, it has been demonstrated that the angular remote sensing signal, in the form of the angular index NDHD, contains information that is complimentary to that of traditional

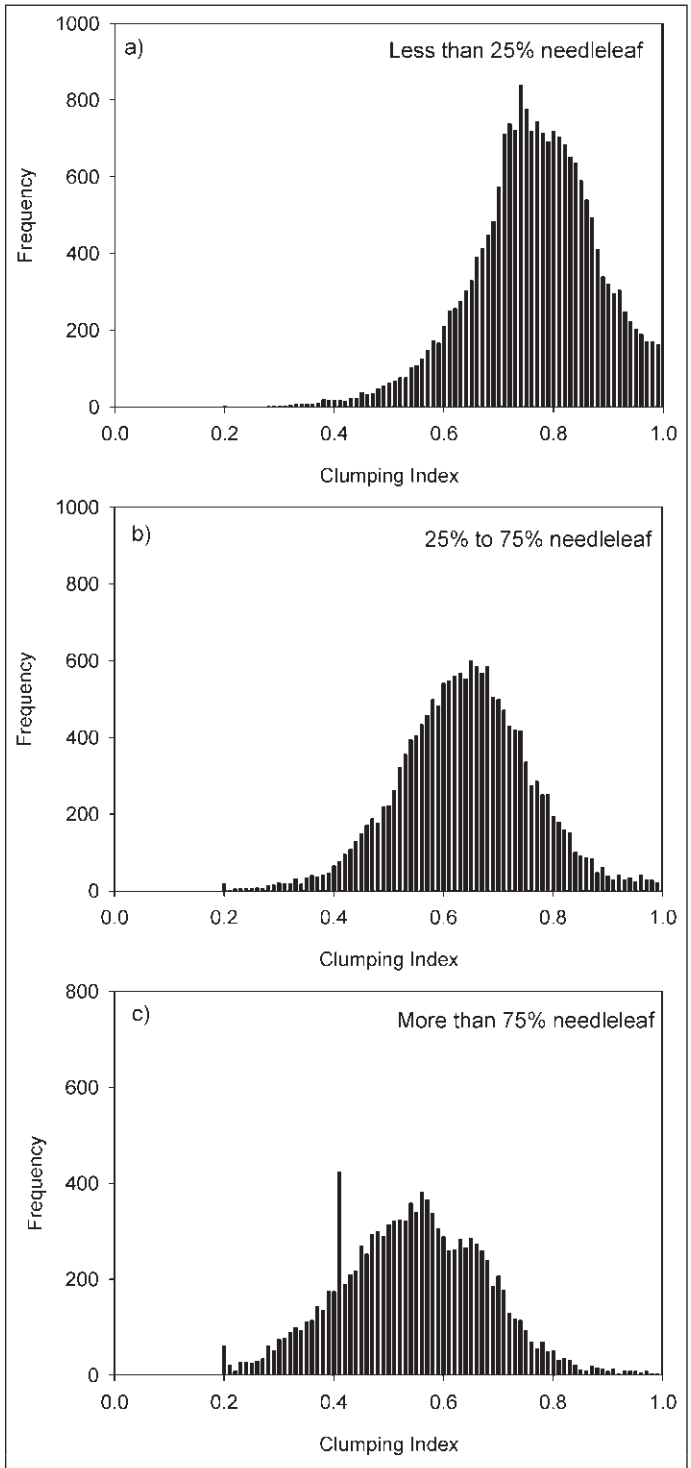

Figure 8. Clumping index histograms for different percentages of needleleaf species in the 7 km by 7 km pixels: (a) less than 25%, (b) between 25% and 75%, and (c) more than 75%.

Table 4. Mean retrieved clumping index and field measurement range of clumping index for each vegetated cover type.

Most frequently occurring cover type in 7 km × 7 km	Mean clumping index from POLDER	In situ clumping index	References for in situ clumping index
Closed evergreen forest	0.56	0.30–0.70	Chen et al., 1997; Leblanc et al., 2005
Closed deciduous forest	0.72	0.65–0.95	Chen et al., 1997; Leblanc and Chen, 2001
Closed mixed evergreen–deciduous forest	0.66	0.60–0.80	Unpublished data from sites in Chen et al., 2002
Open evergreen forest	0.61	0.25–0.80	Chen et al., 1997; Leblanc et al., 2005
Open mixed evergreen–deciduous forest	0.80	0.60–0.75	Unpublished data from sites in Chen et al., 2002
Herbaceous vegetation	0.88	0.70–0.95	Unpublished data from sites in Chen et al., 2002
Wetland	0.76	—	
Annual graminoid	0.91	0.70–0.95	Unpublished data from sites in Chen et al., 2002
Sparse vegetation	0.67	—	

Note: The classes are based on the most frequently occurring cover types based on SPOT VEGETATION classification (Cihlar et al., 2002).

vegetation indices such as the NDVI. Based on the simulated NDHD – clumping index relationships for different cover types, directional reflectance data were used to map the foliage clumping index over Canada. Although the map shown here has a low resolution with about 30% error, it gives a clumping index spatial distribution and can be used in carbon modelling to estimate the spatial distribution within cover types (Chen et al., 2003), which is an improvement over using fixed clumping index values for given cover types (Liu et al., 1999; 2002). An approach similar to that presented here is also being used to map the clumping index at the global scale (Chen et al., 2005), in which other considerations specific to global mapping are introduced.

Acknowledgements

The authors would like to thank Richard Fernandes and Robert Fraser who reviewed the manuscript before submission, the two anonymous reviewers for their constructive comments, and Josef Cihlar for supporting multiangular reflectance and foliage structure retrieval research over the years.

References

Asner, G P. 2000. Contribution of multi-view angle remote sensing to land-surface and biogeochemical research. *Remote Sensing Reviews*, Vol. 18, pp. 137–165.

Barnsley, M.J., Lewis, P., O'Dwyer, S., Disney, M.I., Hobson, P., Cutter, M., and Lobb, D. 2000. On the potential of CHRIS/PROBA for estimating vegetation canopy properties from space. *Remote Sensing Reviews*, Vol. 19, pp. 171–189.

Bicheron, P., and Leroy, M. 1999. A method of biophysical parameter retrieval at global scale by inversion of a vegetation reflectance model. *Remote Sensing of Environment*, Vol. 67, pp. 251–266.

Chen, J.M., and Cihlar, J. 1995. Plant canopy gap-size analysis theory for improving optical measurements of leaf area index. *Applied Optics*, Vol. 34, pp. 6211–6222.

Chen, J.M., and Cihlar, J. 1996. Retrieving leaf area index of boreal conifer forests using Landsat TM images. *Remote Sensing of Environment*, Vol. 55, No. 2, pp. 153–162.

Chen, J.M., and Leblanc, S.G. 1997. A four-scale bidirectional reflectance model based on canopy architecture. *IEEE Transactions on Geoscience and Remote Sensing*, Vol. 35, pp. 1316–1337.

Chen, J.M., and Leblanc, S.G. 2001. Multiple-scattering scheme useful for geometric optical modelling. *IEEE Transactions on Geoscience and Remote Sensing*, Vol. 39, pp. 1061–1071.

Chen, J.M., Rich, P.M., Gower, T.S., Norman, J.M., and Plummer, S. 1997. Leaf area index of boreal forests: theory, techniques and measurements. *Journal of Geophysical Research*, Vol. 102, pp. 29 429 – 29 444.

Chen, J.M., Lacaze, R., Leblanc, S.G., Roujean, J.-L., and Liu, J. 1999a. POLDER BRDF and photosynthesis: an angular signature useful for ecological applications. In *Proceedings of the 2nd International Workshop on Multiangular Measurements and Models*, 15–17 September 1999, Ispra, Italy. Abstract. JRC, Ispra, Italy. p. 98.

Chen, J.M., Liu, J., Cihlar, J., and Goulden, M.L. 1999b. Daily canopy photosynthesis model through temporal and spatial scaling for remote sensing applications. *Ecological Modelling*, Vol. 124, pp. 99–119.

Chen, J.M., Pavlic, G., Brown, L., Cihlar, J., Leblanc, S.G., White, H.P., Hall, R.J., Peddle, D., King, D.J., Trofymow, J.A., Swift, E., Van der Sanden, J., and Pellikka, P. 2002. Derivation and validation of Canada-wide coarse-resolution leaf area index maps using high resolution satellite imagery and ground measurements. *Remote Sensing of Environment*, Vol. 80, pp. 165–184.

Chen, J.M., Liu, J., Leblanc, S.G., Lacaze, R., and Roujean, J.-L. 2003. A demonstration of the utility of multi-angle remote sensing for estimating carbon absorption by vegetation. *Remote Sensing of Environment*, Vol. 84, pp. 516–525.

Chen, J.M., Menges, C.H., and Leblanc, S.G. 2005. Global mapping of the foliage clumping index using multi-angular satellite data. *Remote Sensing of Environment*, Vol. 97, No. 4, pp. 447–457.

Cihlar, J., Beaubien, J., and Latifovic, R. 2002. *Land cover of Canada 1998*. Special Publication, NBIOME Project. Canada Centre for Remote Sensing, Ottawa, Ont.

Dawson, T.P., Curran, P.J., and Plummer, S.E. 1998. LIBERTY — modelling the effects of leaf biochemistry on reflectance spectra. *Remote Sensing of Environment*, Vol. 65, pp 50–60.

Deschamps, P.Y., Bréon, F.M., Leroy, M., Podaire, A., Bricaud, A., Buriez, J.C., and Sèze, G. 1994. The POLDER mission: instrument characteristics and scientific objectives. *IEEE Transactions on Geoscience and Remote Sensing*, Vol. 32, pp. 598–615.

Du Pury, D.G.G., and Farquhar, G.D. 1997. Simple scaling of photosynthesis from leaves to canopies without the errors of big-leaf models. *Plant, Cell and Environment*, Vol. 20, pp. 537–557.

Fernandes, R., and Leblanc, S.G. 2005. Parametric (modified least squares) and non-parametric (Theil–Sen) linear regressions for predicting biophysical parameters in the presence of measurement errors. *Remote Sensing of Environment*, Vol. 95, pp. 303–316.

Fernandes, R., Butson, C., Leblanc, S., and Latifovic, R. 2003. Landsat-5 TM and Landsat-7 ETM+ based accuracy assessment of leaf area index products for Canada derived from SPOT-4 VEGETATION data. *Canadian Journal of Remote Sensing*, Vol. 29, No. 2, pp. 241–258.

Fougnie, B., Hagolle, O., and Cabot, F. 2001. In-flight measurement and correction of non-linearity of the POLDER-1's sensitivity. In *Proceedings of the 8th Symposium of the International Society for Photogrammetry and Remote Sensing*, 8–12 January 2001, Aussois, France. Centre National d'Études Spatiales (CNES), Toulouse, France. pp. 211–219.

Knyazikhin, Y., Martonchik, J.V., Diner, D.J., Myneni, D.J., Verstraete, M.M., Pinty, B., and Godron, N. 1998. Estimation of vegetation canopy leaf area index and fraction of absorbed photosynthetically active radiation from atmosphere-corrected MISR data. *Journal of Geophysical Research*, Vol. 103, pp. 32 239 – 32 256.

Kucharik, C.J., Norman, J.M., Murdock, L.M., and Gower, S.T. 1997. Characterizing canopy nonrandomness with a multiband vegetation imager (MVI). *Journal of Geophysical Research*, Vol. 102, pp. 29 455 – 29 473.

Lacaze, R. 1999. *Restitution des paramètres des surfaces continentales utiles à l'étude du climat à partir des observations multiangulaires de la télédétection optique*. Ph.D. thesis, Université Toulouse III (Paul Sabatier), Toulouse, France. 236 pp.

Lacaze, R., Chen, J.M., Roujean, J.-L., and Leblanc, S.G. 2002. Retrieval of vegetation clumping index using hot spot signatures measured by POLDER instrument. *Remote Sensing of Environment*, Vol. 79, pp. 84–95

Lang, A.R.G., and Xiang, Y. 1986. Estimation of leaf area index from transmission of direct sunlight in discontinuous canopies. *Agricultural and Forest Meteorology*, Vol. 35, pp. 229–243.

Leblanc, S.G. 2002. Correction to the plant canopy gap size analysis theory used by the tracing radiation and architecture of canopies (TRAC) instrument. *Applied Optics*, Vol. 31, pp. 7667–7670.

Leblanc, S.G., and Chen, J.M. 2000. A Windows graphic interface (GUI) for the Five-Scale model for fast BRDF simulations. *Remote Sensing Reviews*, Vol. 19, pp. 293–305.

Leblanc, S.G., and Chen, J.M. 2001. A practical scheme for correcting multiple scattering effects on optical LAI measurements. *Agricultural and Forest Meteorology*, Vol. 110, pp. 125–139.

Leblanc, S.G., Bicheron, P., Chen, J.M., Leroy, M., and Cihlar, J. 1999. Investigation of directional reflectance in boreal forests using an improved 4-scale model and airborne POLDER data. *IEEE Transactions on Geoscience and Remote Sensing*, Vol. 37, No. 3, pp. 1396–1414.

Leblanc, S.G., Chen, J.M., White, H.P., Cihlar, J., Lacaze, R., Roujean, J.-L., and Latifovic, R. 2001. Mapping vegetation clumping index from directional satellite measurements. In *Proceedings of the 8th Symposium of the International Society for Photogrammetry and Remote Sensing*, 8–12 January 2001, Aussois, France. Centre National d'Études Spatiales (CNES), Toulouse, France. pp. 450–459.

Leblanc, S.G., Chen, J.M., White, H.P., Latifovic, R., Fernandes, R., Roujean, J.-L., and Lacaze, R. 2002. Mapping leaf area index heterogeneity over Canada using directional reflectance and anisotropy models. In *IGARSS 2002, Proceedings of the IEEE International Geoscience and Remote Sensing Symposium*, 24–28 June 2002, Toronto, Ont. CD-ROM. IEEE, Piscataway, N.J.

Leblanc, S.G., Chen, J.M., Fernandes, R., Deering, D.W., and Conley, A. 2005. Methodology comparison for canopy structure parameters extraction from digital hemispherical photography in boreal forests. *Agricultural and Forest Meteorology*, Vol. 129, pp. 187–207.

Leroy, M., Deuze, J.L., Bréon, F.M., Hautecoeur, O., Herman, M., Buriez, J.C., Tanre, D., Bouffies, S., Chazette, P., and Roujean, J.L. 1997. Retrieval of atmospheric properties and surface bidirectional reflectances over the land from POLDER. *Journal of Geophysical Research*, Vol. 102, pp. 17 023 – 17 037.

Liu, J., Chen, J.M., Cihlar, J., and Park, W.M. 1997. A process-based boreal ecosystem productivity simulator using remote sensing inputs. *Remote Sensing of Environment*, Vol. 62, pp. 158–175.

Liu, J., Chen, J.M., Cihlar, J., and Chen, W. 1999. Net primary productivity distribution in the BOREAS study region from a process model driven by satellite and surface data. *Journal of Geophysical Research*, Vol. 104, No. D22, pp. 27 735 – 27 754.

Liu, J., Chen, J.M., Cihlar, J., and Chen, W. 2002. Remote sensing based estimation of net primary productivity over Canadian landmass. *Global Ecology and Biogeography*, Vol. 11, pp.115–129.

Myneni, R.B., Nemani, R.R., and Running, E.W. 1997. Algorithm for the estimation of global land cover, LAI and FPAR based on radiative transfer models. *IEEE Transactions on Geoscience and Remote Sensing*, Vol. 35, pp. 1380–1393.

Nilson, T. 1971. A theoretical analysis of the frequency of gaps in plant stands. *Agricultural Meteorology*, Vol. 8, pp. 25–38.

Nolin, A.W., Fetterer, F.M., and Scambos, T.A. 2002. Surface roughness characterizations of sea ice and ice sheets: case studies with MISR data. *IEEE Transactions on Geoscience and Remote Sensing*, Vol. 40, pp. 1605–1615.

Norman, J.M. 1993. Scaling processed between leaf and canopy levels. In *Scaling physiological processes: leaf to globe*. Edited by J.R. Ehleringer and C.B. Field. Academic Press, San Diego, Calif. pp. 41–76.

Pavlic, G., Fernandes, R., Chen, W., Fraser, R., and Leblanc, S.G. 2002. Canada wide geo-spatial datasets in support of environmental monitoring and modelling. In *Proceedings of ISPRS Technical Commission IV Symposium, Joint International Symposium on Geospatial Theory, Processing and Applications*, 9–12 July 2002, Ottawa, Ont. CD-ROM. ISRSE Office of the Secretariat, Tucson, Ariz.

Pinty, B., Widlowski, J.-L., Godron, N., Verstraete, M.M., and Diner, D.J. 2001. Uniqueness of multiangular measurements — Part 1: an indicator of subpixel surface heterogeneity from MISR. *IEEE Transactions on Geoscience and Remote Sensing*, Vol. 40, pp. 1559–1573.

Press, W., Teukolsky, S., Vetterling, W., and Flannery, B. 1994. *Numerical recipes in C*. Cambridge University Press, Cambridge, UK. 994 pp.

Privette, J.L., Myneni, R.B., Knyazikhin, Y., Mukufute, M., Roberts, G., Tian Y., Wang, Y., and Leblanc, S.G. 2002. Early spatial and temporal validation of MODIS LAI product in Africa. *Remote Sensing of Environment*, Vol. 83, pp. 232–243.

Roujean, J.L., and Lacaze, R., 2002. A global mapping of vegetation parameters from POLDER multi-angular measurements for surface–atmosphere interaction studies: a pragmatic approach and its validation. *Journal of Geophysical Research*, Vol. 107, No. D12, pp. 1029–1042.

Sandmeier, St., Muller, Ch., Hosgood, B., and Andreoli, G. 1998. Physical mechanisms in hyperspectral BRDF data of grass and watercress. *Remote Sensing of Environment*, Vol. 66, pp. 222–233.

Walter, J.-M.N., Fournier, R.A., Soudani, K., and Meyer, E. 2003. Integrating clumping effects in forest canopy structure: an assessment through hemispherical photographs. *Canadian Journal of Remote Sensing*, Vol. 29, No. 3, pp. 388–410.

Wang, Y.-P., and Leuning, R. 1998. A two-leaf model for canopy conductance, photosynthesis and partitioning of available energy: I. Model description and comparison with a multi-layered model. *Agricultural and Forest Meteorology*, Vol. 91, pp. 89–111.

White, H.P., Leblanc, S.G., Chen, J.M., Lacaze, R., and Roujean, J.-L. 2001a. Mapping biophysical parameters with modeled and inverted functions from directional satellite measurements. In *Proceedings of the 23rd Canadian Symposium on Remote Sensing*, 21–24 August 2001, Québec City, Que. Canadian Aeronautics and Space Institute (CASI), Ottawa, Ont. pp. 407–414.

White, H.P., Miller, J.R., and Chen, J.M. 2001b. Four-Scale linear model for anisotropic reflectance (FLAIR) for plant canopies — Part I: Model description and partial validation. *IEEE Transactions on Geoscience and Remote Sensing*, Vol. 39, pp. 1072–1083.

White, H.P., Miller, J.R., and Chen, J.M. 2002. Four-Scale linear model for anisotropic reflectance (FLAIR) for plant canopies — Part II: Validation and inversion with CASI, POLDER, and PARABOLA data at BOREAS. *IEEE Transactions on Geoscience and Remote Sensing*, Vol. 40, pp. 1038–1046.

Widlowski, J.-L., Pinty, B., Godron, N., Verstraete, M.M., and Davis, B. 2001. Characterization of surface heterogeneity detected at the MIRS/TERRA subpixel scale. *Geophysical Research Letters*, Vol. 28, pp. 4639–4642.